The palmitoyltransferase Approximated promotes growth via the Hippo pathway by palmitoylation of Fat

Hitoshi Matakatsu,[1,2] Seth S. Blair,[2] and Richard G. Fehon[1]

[1]Department of Molecular Genetics and Cell Biology, University of Chicago, Chicago, IL 60637
[2]Department of Zoology, University of Wisconsin, Madison, WI 53706

The large protocadherin Fat functions to promote Hippo pathway activity in restricting tissue growth. Loss of Fat leads to accumulation of the atypical myosin Dachs at the apical junctional region, which in turn promotes growth by inhibiting Warts. We previously identified Approximated (App), a DHHC domain palmitoyltransferase, as a negative regulator of Fat signaling in growth control. We show here that App promotes growth by palmitoylating the intracellular domain of Fat, and that palmitoylation negatively regulates Fat function. Independently, App also recruits Dachs to the apical junctional region through protein–protein association, thereby stimulating Dachs's activity in promoting growth. Further, we show that palmitoylation by App functions antagonistically to phosphorylation by Discs-overgrown, which activates Fat. Together, these findings suggest a model in which App promotes Dachs activity by simultaneously repressing Fat via posttranslational modification and recruiting Dachs to the apical junctional region, thereby promoting tissue growth.

Introduction

A central question in developmental biology is how overall size and cell number in an organ are regulated during normal development, particularly in tissues that display endogenous size regulation. Recent studies have revealed the existence of the Hippo pathway that appears to coordinate developmental patterning, proliferation, apoptosis, and cell growth to regulate overall organ size (Halder and Johnson, 2011; Boggiano and Fehon, 2012; Staley and Irvine, 2012; Enderle and McNeill, 2013; Hariharan, 2015). At the core of this pathway are two kinases, Hippo and Warts (Wts), and the scaffold proteins Salvador (Sav) and Mats. Downstream of these core components is the transcriptional coactivator Yorkie (Yki), which promotes expression of cell proliferation and anti-apoptotic genes. Phosphorylation by Wts inactivates Yki, thereby restricting tissue growth. Thus, loss of any of the core components leads to increased proliferation, reduced apoptosis, and tissue overgrowth.

It is still not entirely clear how input from upstream of the core components regulates Hippo pathway activity and growth. Three proteins, Expanded (Ex), Merlin, and Kibra, are proposed to form a complex at the apical junctional region (AJR) to regulate activity of the core kinases (Hamaratoglu et al., 2006; Baumgartner et al., 2010; Genevet et al., 2010; Yu et al., 2010). Ex also associates directly with Yki and is believed to sequester Yki at the AJR (Badouel et al., 2009). The transmembrane proteins Echinoid and Crumbs bind Sav and Ex, respectively (Ling et al., 2010; Yue et al., 2012). Loss of any of these proteins causes nuclear accumulation of Yki, transcriptional up-regulation of Yki target genes, and overgrowth.

Another transmembrane protein that is believed to function upstream in the Hippo pathway is Fat (Ft), which encodes a giant protocadherin (Bennett and Harvey, 2006; Cho et al., 2006; Silva et al., 2006; Willecke et al., 2006). Ft binds in a heterophilic manner to another giant protocadherin, Dachsous (Ds), and *ft* mutants display not only imaginal tissue overgrowth, but also disruption in planar cell polarity (PCP; Blair, 2012; Thomas and Strutt, 2012; Lawrence and Casal, 2013; Matis and Axelrod, 2013; Carvajal-Gonzalez and Mlodzik, 2014). Loss of Ft leads to accumulation of the atypical myosin Dachs at the AJR, and genetic epistasis data suggest that *ft* controls growth through *dachs*, suggesting that Ft restricts tissue growth by regulating the amount of Dachs at the AJR (Mao et al., 2006; Rogulja et al., 2008). How Dachs regulates growth is not yet entirely clear, although it is known to alter the conformation of Wts and promote its destabilization (Cho et al., 2006; Vrabioiu and Struhl, 2015).

Other upstream pathway components are thought to work with Ft to regulate the localization or accumulation of Dachs at the AJR. Fbxl7 encodes an F-box domain protein, which binds to the Ft intracellular domain (ICD; Bosch et al., 2014; Rodrigues-Campos and Thompson, 2014). Although the function of Fbxl7 is still not clear, Fbxl7 might destabilize Dachs by

Correspondence to Richard G. Fehon: rfehon@uchicago.edu

Abbreviations used: AJR, apical junctional region; CK, Casein kinase; ICD, intracellular domain; PCP, planar cell polarity.

The Rockefeller University Press $30.00
J. Cell Biol. Vol. 216 No. 1 265–277
https://doi.org/10.1083/jcb.201609094

ubiquitination, because F-box proteins often act as E3 ubiquitin ligases. Disc-overgrown (Dco) encodes a Casein kinase 1ε (CK1ε). Dco binds to and phosphorylates the Ft ICD (Feng and Irvine, 2009; Sopko et al., 2009), and loss of Dco leads to overgrowth in imaginal discs (Zilian et al., 1999), suggesting that Dco activates Ft by phosphorylating its ICD. Consistent with this idea, mutations in Dco phosphorylation target sites partially suppress the ability of Ft to repress growth (Pan et al., 2013). Phosphorylation of the Ft ICD is also influenced by Ds and by changes in Ft-Ds binding mediated by the Golgi-retained kinase Four-joined, indicating that interactions mediated by the extracellular domain influence activity of the ICD (Feng and Irvine, 2009; Sopko et al., 2009).

In contrast to Fbxl7 and Dco, Approximated (App) functions antagonistically to Ft in growth control and Dachs regulation (Matakatsu and Blair, 2008). *app* mutants display reduced wing size and strongly suppress the *ft* overgrowth phenotype. Loss of App also causes decreased accumulation of ectopically expressed Dachs at the AJR, suggesting that App promotes recruitment of Dachs to the plasma membrane. Interestingly, App encodes a member of the DHHC family of palmitoyltransferases, proteins that catalyze the addition of palmitoyl lipid groups to proteins at cysteine residues (Linder and Deschenes, 2007; Fukata and Fukata, 2010). These observations have led to the proposal that App-mediated palmitoylation of Dachs might promote its membrane association (Matakatsu and Blair, 2008). However, other myosins are not known to be palmitoylated, and Dachs does not contain strong consensus palmitoylation sites (Matakatsu and Blair, 2008).

We show here that App palmitoylates the intracellular domain of Ft, thereby repressing the ability of Ft to control growth. Consistent with previous work showing that Ft regulates growth through Dachs, we found that loss of App results in reduction of endogenously expressed Dachs at the AJR. Interestingly, our results indicate that this decreased Dachs accumulation is only partially caused by increased Ft activity. In addition, we show that App promotes Dachs accumulation at the AJR and growth independently of Ft and palmitoylation, possibly by interacting with Dachs. We also demonstrate that App functions antagonistically to Dco, which activates Ft by phosphorylating its cytoplasmic tail. Together, these findings provide a novel model for how posttranslational modifications mediated by App and Dco function to regulate levels of Ft signaling and control tissue growth.

Results

Ft, Dco, and App regulate the subcellular localization of Dachs

To better understand relationship between Ft, Dco, App, and Dachs, we generated two antisera against Dachs, one specific for the N-terminal extension domain (aa 1–280) and the other for the C-terminal tail domain (aa 1,013–1,232). Dachs immunostaining using either antibody was lost in d^{GC13} mutant clones (Fig. S1, B and C), indicating that these antisera are specific to Dachs. Dachs staining in the imaginal wing epithelium was predominantly localized at the AJR, consistent with previous studies using Dachs transgenes (Mao et al., 2006; Matakatsu and Blair, 2008; Ambegaonkar et al., 2012; Bosveld et al., 2012; Brittle et al., 2012). In *ft* and *dco* mutant clones, Dachs staining was dramatically increased at the AJR (Fig. 1, A–D; and Fig. S1, D–I), but optical sections taken more basally showed only a slight increase in Dachs staining (Mao et al., 2006; Fig. 1, B and D). In contrast, ectopically expressed Dachs in wild-type cells was enriched not only at the AJR, but also more basally (Fig. S1, D–F). Collectively, these observations suggest that Dco and Ft function to regulate Dachs specifically at the AJR.

Our previous data suggest that App acts to promote AJR localization and activity of Dachs (Matakatsu and Blair, 2008). Using these Dachs antisera, we confirmed that Dachs staining is reduced at apical cell membrane in *app* null mitotic clones (Fig. 1 E). Interestingly, Dachs staining also is increased throughout the basal cytoplasm in *app* mutant clones (Fig. 1 F), suggesting that Dachs protein might be more abundant in the absence of App function. To test this possibility, we compared immunoblots of Dachs from wild-type and app^{-} imaginal tissue and found increased Dachs in *app* mutants (Fig. 1, H and I). Collectively, these results suggest that (a) Dachs must localize to the AJR to promote growth, and (b) because loss of App affects both the localization and abundance of Dachs, these Dachs properties might be linked in imaginal tissues.

Regulation of Dachs requires the DHHC motif in App

App encodes a four-pass transmembrane protein containing a DHHC cysteine-rich domain (Fig. 2 A), the catalytic domain in proteins that function as palmitoyltransferases (Fukata and Fukata, 2010). However, App has never been shown to have palmitoyltransferase activity. Previous studies have shown that mutating cysteine to serine (DHHS) or histidine to alanine (DAHC) in the DHHC motif abolishes palmitoyltransferase activity in vivo and in vitro (Lobo et al., 2002; Roth et al., 2002; Mitchell et al., 2010). Therefore, we generated three point mutants, app^{DHHS}, app^{DAHC}, and $app^{DHH\Delta C}$, in the *app* locus using the CRISPR-Cas9 system (Figs. 2 A and S2, A and B). All three mutations in the DHHC motif were homozygous viable (Table S1) and displayed slight undergrowth, weak proximodistal shortening in the wing and leg, and planar cell polarity defects, characteristic phenotypes of *app* null mutants (Fig. 2, C–F; and Fig. S2, C–H).

To better understand the effects of mutations in the DHHC motif on App function, we examined homozygous app^{DHHS} mitotic clones in the third-instar imaginal epithelium. app^{DHHS} clones showed decreased App accumulation at the AJR (Fig. 2, L and M). Although Dachs staining was severely disrupted in *app* null mutants (Fig. 1, E–G), in app^{DHHS} clones Dachs was reduced but not absent from the AJR (Fig. 2, N and O), suggesting a palmitoylation-independent role for App in Dachs localization. Similar results were seen with the other DHHC mutant alleles (unpublished data).

To further test the function of the DHHC motif, we next examined the effect of Gal4/UAS-driven overexpression of wild-type and mutant forms of App. Expression of wild-type App resulted in slightly reduced wing size, whereas expression of either *UAS-*app^{DHHS} or *UAS-*app^{DAHC} resulted in stronger, *app*-like undergrowth (Fig. 2, G–I and K). In the imaginal epithelium, expression of wild-type App induced slightly higher accumulation of Dachs at the AJR and also reduction of Dachs in the basal cytoplasm (Fig. 2, R and S). In contrast, ectopic expression of the DHHC motif mutant *UAS-*app^{DHHS} or *UAS-*app^{DAHC} in the posterior compartment using *hh-Gal4* caused dramatically decreased AJR localization of Dachs and increased basal accumulation (Fig. 2, T and U), suggesting a dominant-negative effect. Because

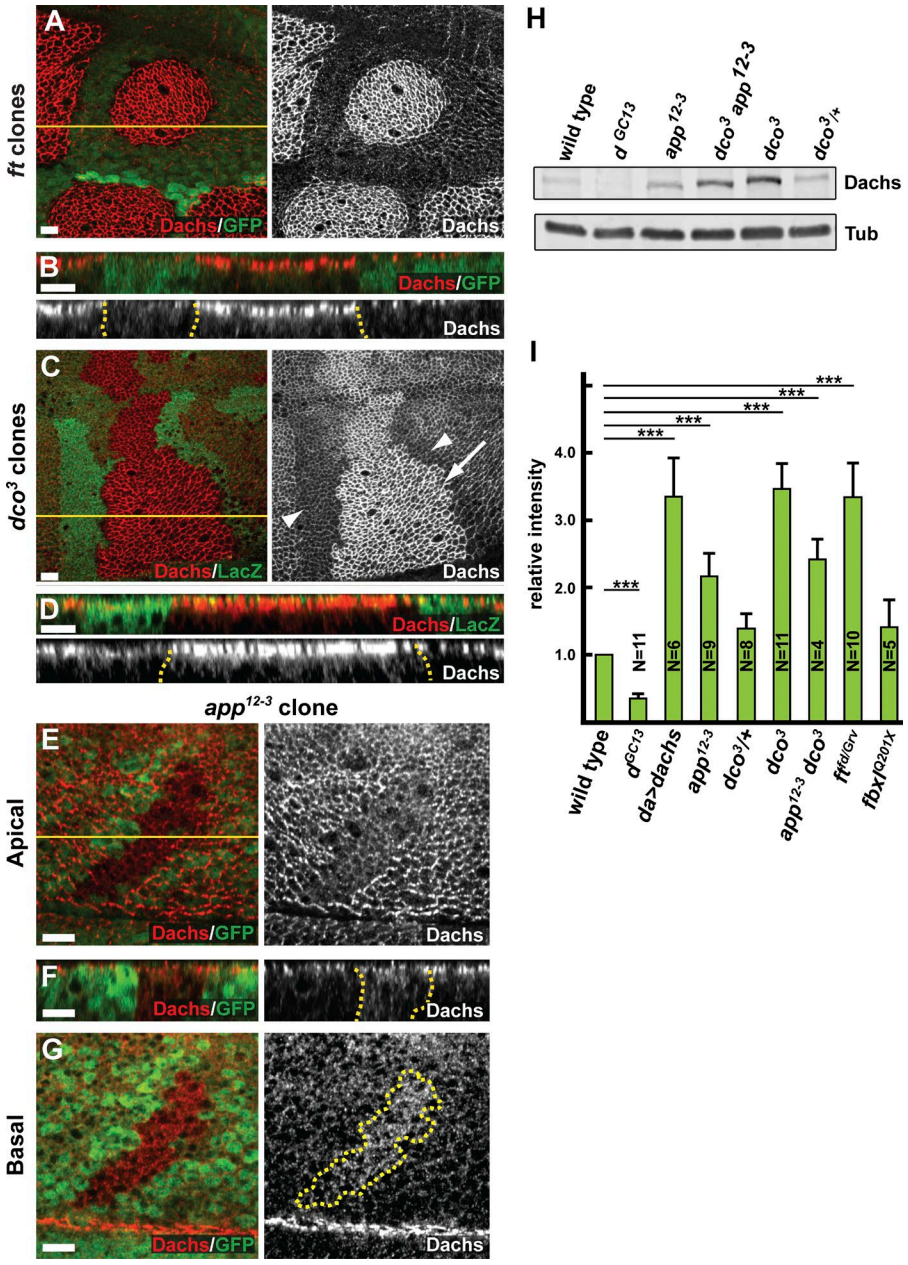

Figure 1. **App promotes the localization of Dachs to AJR.** (A–G) The localization and level of anti-Dachs staining in ft^{fd} (A and B), dco^3 (C and D), and app^{12-3} (E–G) mitotic clones, marked by the absence of GFP (A, B, and E–G) or anti-LacZ (C and D) staining. Anti-Dachs staining is increased in ft^{fd} (A and B) and dco^3 (C and D; arrow in C indicates mutant cells) mitotic clones at the AJR. In +/+ sister clones (C, arrowheads), anti-Dachs staining is lower than in surrounding dco^3/+ cells. Anti-Dachs staining is reduced apically (E and F) and increased basally (F and G) in app^{12-3} mitotic clones. (H and I) Immunoblot analysis showing Dachs levels in wing imaginal disc cell lysates of the indicated genotypes. Total Dachs is elevated in the app^{12-3} and dco^3 mutants. Quantification of Dachs levels from similar immunoblots shows that Dachs levels, normalized with anti-αTubulin (Tub), are also up-regulated in *ft* mutants compared with wild type. Error bars are mean ± SEM. ***, $P < 0.001$ (two-tailed paired Student's *t* test between wild type and each genotype). Dotted yellow lines in this and subsequent figures denote the boundary of somatic mosaic mutant clones or Gal4 expression, whereas solid yellow lines indicate the position of optical cross sections in the panels immediately below. Bars, 5 µm.

ectopic expression of the DHHC mutant alleles in an *app* null background also reduced Dachs accumulation in the posterior compartment, it is possible that this dominant-negative effect is caused not only by interference with App but additionally by an influence on Ft activity (Fig. S3, E–H). However, although ectopic expression of wild-type App in a *ft* mutant background promoted Dachs accumulation at the AJR, expression of the DHHC alleles did not (Fig. S3, I–L), indicating that App palmitoyltransferase activity is important in the absence of Ft. Indeed, our recent studies have identified an additional target for App, an SH3 domain–containing protein named Dlish (Zhang et al., 2016).

To ask whether the growth defects of *app* mutants are caused by alterations in Hippo pathway output, we used the *ex-lacZ* and *fj-lacZ* reporters, which are responsive to Yki activity downstream of the Hippo pathway. app^{12-3} null clones result in little to no change in expression of *ex-lacZ* (Fig. S3 M), nor did we detect an effect of app^{DHHS} mutant clones on expression of the *fj-lacZ* reporter (Fig. 2 W). This likely reflects the relatively weak effect of *app* loss on Yki function when Ft is present. In contrast, the app^{DHHS} mutation strongly suppressed up-regulation of the *fj-lacZ* reporter in *ft* mutant clones in the hinge region of the wing imaginal disc, though this effect was less obvious in the blade where *fj-lacZ* expression is normally quite high (Fig. 2 X, compare with V). Unlike wild-type *app*, ectopic expression of *UAS-*app^{DHHS} did cause noticeably decreased *ex-lacZ* expression, consistent with the stronger undergrowth seen in the adult wing (Figs. 2 H and S3 P). These results indicate that the effect of *app* mutations on tissue growth is mediated through the Hippo pathway, and again suggest that App can act independently of Ft, given that mutation of the DHHC domain has a phenotype even in a *ft* null mutant background.

Dachs forms a complex with App but is not palmitoylated by App

As the catalytic domain is cytoplasmic in DHHC family members, including App, their targets can be cytoplasmic proteins

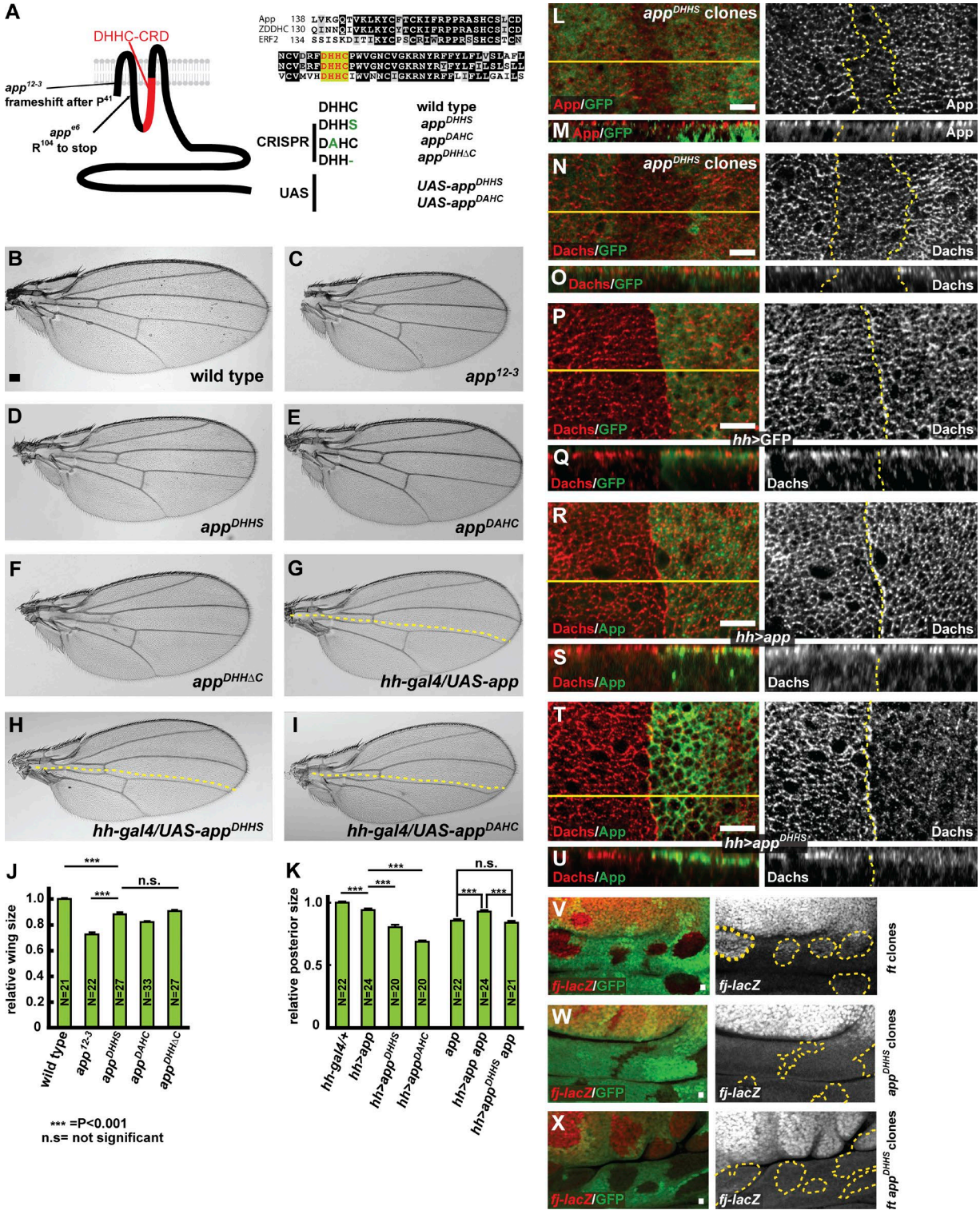

Figure 2. **Mutations in the DHHC motif of *app* affect its role in growth control.** (A) App structure, alignment of DHHC cysteine-rich domains between different palmitoyltransferases, and mutations generated in *app*. The $app^{12\text{-}3}$ and app^{e6} null alleles produce severely truncated products. Two missense mutations in the DHHC motif, app^{DHHS} and app^{DAHC}, were produced via genome editing using CRISPR-Cas9 and as UAS-driven transgenes. A single amino acid deletion in the DHHC motif, $app^{DHH\Delta C}$, was also produced by genome editing. (B–I) Comparison of the effect of different *app* mutations and UAS-transgenes on adult wing size. Animals carrying *app* mutations (C–F) or expressing *app* transgenes expressed in the posterior compartment of the wing under the *hh-gal4* driver (G–I) display reduced wing size (dotted yellow lines indicate approximate position of the anterior–posterior boundary). (J) Quantification of wing size in *app* mutant animals. Wing size is most severely reduced in $app^{12\text{-}3}$, a null mutation, but is also reduced in mutations engineered to disrupt function of the DHHC motif in palmitoylation. (K) Quantification of wing size in wild-type or $app^{12\text{-}3}$ mutant flies expressing *app* transgenes in the posterior compartment. The DHHC domain point mutants display dominant-negative phenotypes when expressed in a wild-type background and fail to rescue $app^{12\text{-}3}$ mutant flies. In J and K, error bars are mean ± SEM. ***, $P < 0.001$ (two-tailed unpaired Student's *t* test). n.s., not significant. (L–O) Anti-App (L and M) and anti-Dachs (N and O) staining in app^{DHHS} mitotic clones. Junctional accumulation of both proteins appears slightly reduced in these cells. (P–U) Anti-Dachs

or the intracellular domain of transmembrane proteins. App is predominantly localized at AJR, where other Ft signaling components including Ft, Ds, and Dachs are concentrated (Ma et al., 2003; Matakatsu and Blair, 2008). Although loss of *app* does not affect the localization and abundance of Ft and Ds (Matakatsu and Blair, 2008), Dachs localization is disrupted in *app* mutant cells (Fig. 1, E–G). We considered two nonexclusive possible mechanisms by which App could help recruit Dachs to the AJR: (a) by forming a complex with Dachs or (b) by promoting Dachs membrane association through palmitoylation.

To test these possibilities, we first asked whether App and Dachs could form a complex. When Dachs and App were expressed in S2 cells, Dachs coimmunoprecipitated with App (Fig. 3 A). Dachs also coimmunoprecipitated with App^{DHHS} and App^{DAHC}, indicating that mutation of the DHHC motif did not disrupt the overall structure of App or its association with Dachs.

If App and Dachs form a complex in cells, then removal of Dachs might be expected to affect App localization. We examined App localization in imaginal discs containing *dachs* mutant clones and found that App staining decreased at the AJR and increased basally (Fig. 3, B and C), indicating that these proteins are interdependent for normal localization.

Next we tested the possibility that Dachs is palmitoylated in vivo using a previously described biochemical assay for palmitoylation (Drisdel and Green, 2004; Drisdel et al., 2006). We used Gilgamesh (Gish; a CK1γ) and App as positive controls for this assay, because it is known that CK1 in yeast and DHHC family members are often palmitoylated (Roth et al., 2002). When we expressed Myc-tagged Gish or GFP-tagged App using *da-gal4* in the imaginal epithelium, both proteins were positive for palmitoylation in this assay (Fig. 3 D). In contrast, we could not detect palmitoylation of Dachs in the same experimental assay, suggesting that Dachs is not a target of App enzymatic activity, despite our observation that these proteins form a complex. To independently ask whether Dachs might be palmitoylated, we also mutated a potential Dachs palmitoylation site predicted by CSS-palm 2.0 (Cys763; Fig. S4, A and B; Ren et al., 2008) and two residues (Cys1135 and 1144) in the C-terminal region, which functions in Dachs localization (Zhang et al., 2016). We expressed these mutants as tagged transgenes in the imaginal epithelium and found that none significantly affected the localization or growth-promoting effects of Dachs (Fig. S4, C–M). Together these data strongly argue that Dachs is not palmitoylated by App.

App associates with Ft and promotes its palmitoylation

We considered an additional possibility, that Ft might be a direct target for palmitoylation by App. Previous studies have shown that the cytoplasmic tail of transmembrane proteins can be palmitoylated, and that this modification is often antagonistic to phosphorylation (Salaun et al., 2010). Because Ft has been shown to regulate Dachs localization, we next tested the possibility that Ft is palmitoylated by App. Full-length Ft encodes a 560-kD protocadherin that is cleaved into C-terminal (110-kD) and N-terminal (450-kD) fragments that are covalently linked (Fig. S5, A and B; Feng and Irvine, 2009; Sopko et al., 2009). The C-terminal fragment contains a small part of the extracellular region, the transmembrane domain, and the entire intracellular domain (we refer to this fragment as Ft-ICD).

To ask whether the Ft intracellular domain can be palmitoylated in S2 cells, we first used a Ft expression construct that removes most of the extracellular domain, Ft$^{\Delta ECD}$ (Matakatsu and Blair, 2006). Ft$^{\Delta ECD}$ runs as multiple bands on immunoblots because the Ft intracellular domain is phosphorylated by the CK1ε orthologue, Dco (Feng and Irvine, 2009; Sopko et al., 2009). Accordingly, in our immunoprecipitation experiments, we used lambda phosphatase treatment to resolve Ft to a single band. When App was immunoprecipitated from S2 cells, we observed that coexpressed Ft$^{\Delta ECD}$ was coprecipitated, suggesting that they can form a complex in cells (Fig. 4 A).

To determine whether Ft is palmitoylated, we first examined Ft$^{\Delta ECD}$ expressed in S2 cells in the presence or absence of coexpressed App. App increases the palmitoylation signal from immunoprecipitated Ft$^{\Delta ECD}$ by approximately 1.8-fold relative to Ft$^{\Delta ECD}$ alone (Fig. 4 B). Additionally, we asked whether mutation of the DHHC catalytic domain prevents App-mediated palmitoylation of Ft by coexpressing either App^{DHHS} or App^{DAHC} and found levels of Ft palmitoylation similar to those of control cells without coexpressed App (Fig. 4 B). Next, we expressed HA-tagged, full-length Ft in the imaginal epithelium using *da-gal4* with or without coexpression of App. In these experiments, we detected palmitoylation of the Ft-ICD when expressed alone in imaginal tissue and observed that palmitoylation increased with coexpression of App (relative level with ectopic App to without, 1.6:1; Fig. 4 C). In addition, loss of *app* reduced, but did not eliminate, Ft-ICD palmitoylation in imaginal tissue (relative level in *app* was 0.75 compared with wild type; Fig. 4 D). Together, these data indicate that App promotes palmitoylation of Ft, although we do not exclude the possibility that other DHHC proteins also palmitoylate Ft.

Palmitoylation occurs at cysteine residues (Linder and Deschenes, 2007), so we next determined which residues in Ft are targets for palmitoylation. There are three intracellular cysteine residues in Ft, at positions 4,623, 4,938, and 4,987. Cys^{4623} is located near the transmembrane domain in a region previously shown to be important in regulating PCP (Fig. 4 E; Matakatsu and Blair, 2012). Cys^{4938} and Cys^{4987} are located in the C and D domains, respectively, close to known Dco binding and phosphorylation target sites (Fig. 4 E; Sopko et al., 2009; Pan et al., 2013). When Ft$^{\Delta ECD}$ and App were coexpressed in S2 cells, we detected a faint, smeared band positive for palmitoylation that comigrated with Ft$^{\Delta ECD}$, indicating that Ft-ICD might be palmitoylated (Fig. S5 C). The smeared bands for both Ft$^{\Delta ECD}$ and palmitoylation could be reduced to a single band by phosphatase treatment (Fig. S5 C), confirming that Ft$^{\Delta ECD}$ can be palmitoylated and indicating that Ft-ICD can be simultaneously phosphorylated and palmitoylated.

staining in *hh-gal4; UAS-GFP* (P and Q), *hh-gal4; UAS-app* (R and S), or *hh-gal4; UAS-app^{DHHS}* (T and U) wing imaginal discs. Cytoplasmic Dachs staining is reduced in cells expressing ectopic App (S, right). In contrast, in cells expressing a DHHC domain mutation, Dachs is reduced apically (T, right) and mislocalized throughout cytoplasm (U, right). (V–X) Comparison of the response of *four-jointed-lacZ* (*fj-lacZ*), a Hippo pathway reporter, in *ft^{fd}*, *app^{DHHS}*, and *ft^{fd}; app^{DHHS}* mitotic clones in the hinge region of the wing imaginal disc, where *fj-lacZ* expression is highly sensitive to Hippo pathway output. Mutant clones are marked by the absence of GFP. *fj-lacZ* is up-regulated in *ft^{fd}* mutant clones (V). In contrast, in *app^{DHHS}* mitotic clones, *fj-lacZ* expression does not change (W). Similarly, *fj-lacZ* was only slightly up-regulated in *ft^{fd}; app^{DHHS}* double mutant mitotic clones (X; compare with V). Bars: (B) 100 µm; (L–X) 5 µm.

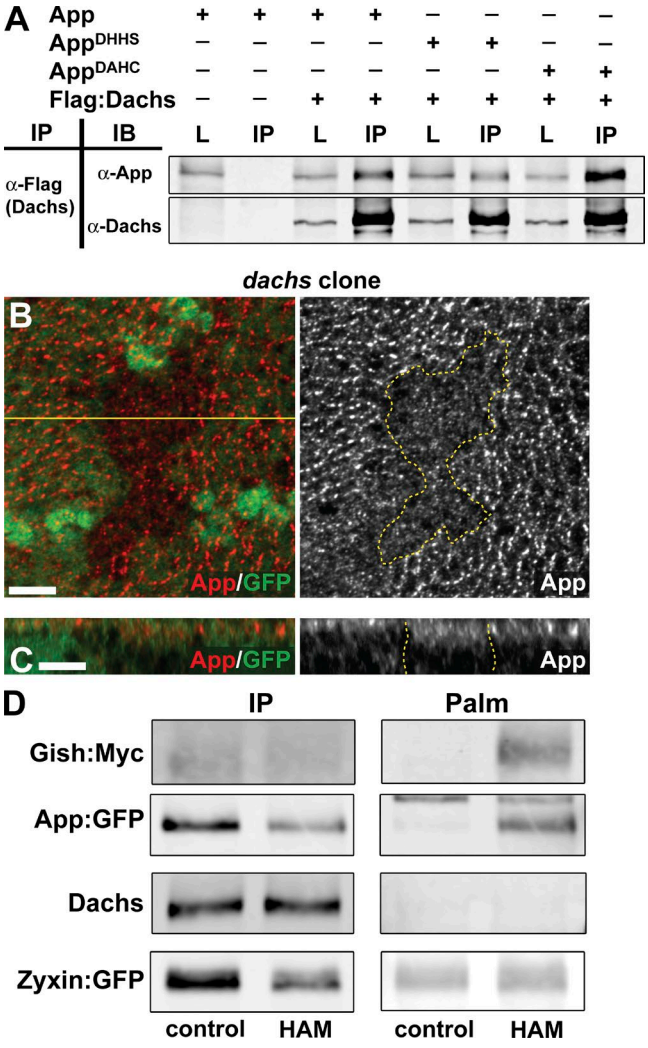

Figure 3. **App forms a complex with Dachs but Dachs is not palmitoylated.** (A) Coimmunoprecipitation between App and Dachs. Flag-tagged Dachs was immunoprecipitated using anti-Flag. Wild-type and DHHC motif mutants coimmunoprecipitate with Dachs in S2 cell lysates. L, total lysates, IP, immunoprecipitates. (B and C) Anti-App staining in *dachs* mitotic clones. Accumulation of App at the AJR is reduced in the absence of Dachs. (D) Palmitoylation assays for transgenically expressed Gish:Myc, App:GFP, endogenous Dachs, and Zyxin:GFP in imaginal tissue. The left column shows immunoprecipitated proteins (IP), and the right column shows palmitoylation (Palm). Control lanes show immunoprecipitations incubated with Tris alone, and HAM immunoprecipitates were treated with hydroxylamine (see Materials and Methods). Dachs and Zyxin:GFP do not show detectable palmitoylation, but Gish:Myc and App:GFP do. Bars, 5 µm.

We next mutated each cysteine residue individually to determine which is responsible for palmitoylation. Mutation of Cys^{4623} ($Ft^{\Delta ECD\text{-}4623C/S}$) displayed detectable palmitoylation when coexpressed with App in S2 cells (Fig. 4 F). However, mutation of either Cys^{4938} ($Ft^{\Delta ECD\text{-}4938C/S}$) or Cys^{4987} ($Ft^{\Delta ECD\text{-}4987C/S}$) slightly diminished detectable palmitoylation (relative levels 0.65 and 0.81, respectively, compared with $Ft^{\Delta ECD\text{-}4623C/S}$), indicating that these cysteine residues might be sites for palmitoylation by App. Consistent with this view, mutation of both Cys^{4938} and Cys^{4987} ($Ft^{\Delta ECD\text{-}2C/S}$) resulted in dramatically reduced palmitoylation (relative level 0.22 compared with $Ft^{\Delta ECD\text{-}4623C/S}$; Fig. 4 F). Mutation of all three intracellular residues had a similar effect on $Ft^{\Delta ECD}$ palmitoylation (Fig. S5 C).

If palmitoylation of the Ft-ICD is important for its function in growth control, then mutation of these cysteine residues should alter Ft function and produce phenotypes similar to loss of *app* function. To test this hypothesis, we used CRISPR-Cas9 to replace the cysteine residues at 4,938 and 4,987 with serine (Fig. S5 D). Flies homozygous for mutations at either cysteine ($ft^{4938C/S}$ or $ft^{4987C/S}$) or doubly homozygous at both ($ft^{2C/S}$) showed reduced wing size, similar to that seen in *app* null mutations (Fig. 4, G–K). The observation that these mutations caused decreased growth indicates that they activate Ft, consistent with the hypothesis that Ft is also activated in *app* null mutants. Together, these results suggest that palmitoylation antagonizes the ability of Ft to negatively regulate Dachs. We note the seemingly paradoxical observation that wing size in the $ft^{2C/S}$ allele is slightly larger than in the $ft^{4987C/S}$ single mutant allele, though we do not currently understand its significance.

Functional interactions between App, Ft, and Dachs

Our previous work indicates that loss of *app* strongly suppresses the *ft* null mutant overgrowth phenotype, producing imaginal discs that are only slightly overgrown (Matakatsu and Blair, 2008). Similarly, although up-regulated in *ft* single mutant clones, *fj-lacZ* expression was normal in *ft app* double mutant clones (Fig. 2, V–X). These results suggest that App can affect growth and Hippo pathway target gene expression even in the absence of Ft. Collectively with our observation that mutation of the DHHC domain in App produces less severe phenotypes than removing App altogether (Fig. 2, D–F and J), these results suggest that App has other functions in addition to Ft palmitoylation.

To further explore the relationship between App and Ft, we examined Dachs localization and levels in cells doubly mutant for *ft* and *app* (*ft; app* cells) in the background of cells singly mutant for either *app* or *ft*. We did this by making somatic mosaic mutant clones of one gene in the background of tissues homozygous for mutations in the other gene (Fig. 5, A–E). Compared with surrounding *app* mutant cells, Dachs in *ft; app* mutant cells appeared highly enriched in the AJR (Fig. 5, A and B). This result indicates that in the absence of both Ft and App, Dachs can still localize to the AJR. It also suggests that with respect to Dachs localization, Ft is epistatic to App, a notion that seems at odds with the observation that with respect to growth *app* strongly suppresses *ft* null phenotypes. However, we found that Dachs level is decreased at the AJR in *ft; app* double mutant cells compared with surrounding *ft* single mutant cells but is increased basally (Fig. 5, C–E). This result clearly indicates that App can promote Dachs localization to the AJR independently of Ft. Because Dachs localization to the AJR correlates well with its function in promoting growth (Mao et al., 2006; Rogulja et al., 2008), it is likely that the Ft-independent effect of App to promote growth is mediated through Dachs.

Dco and App function antagonistically to regulate Ft

Ft activity in growth control is regulated via phosphorylation of its cytoplasmic tail by Dco (Feng and Irvine, 2009; Sopko et al., 2009). Because loss of either Dco or Ft results in overgrowth, Dco mediated phosphorylation is thought to activate Ft, presumably by promoting removal of Dachs from the AJR (Feng and Irvine, 2009; Sopko et al., 2009). Consistent with this idea, Dachs is enriched at the AJR in *dco* mutant clones (Fig. 1, C

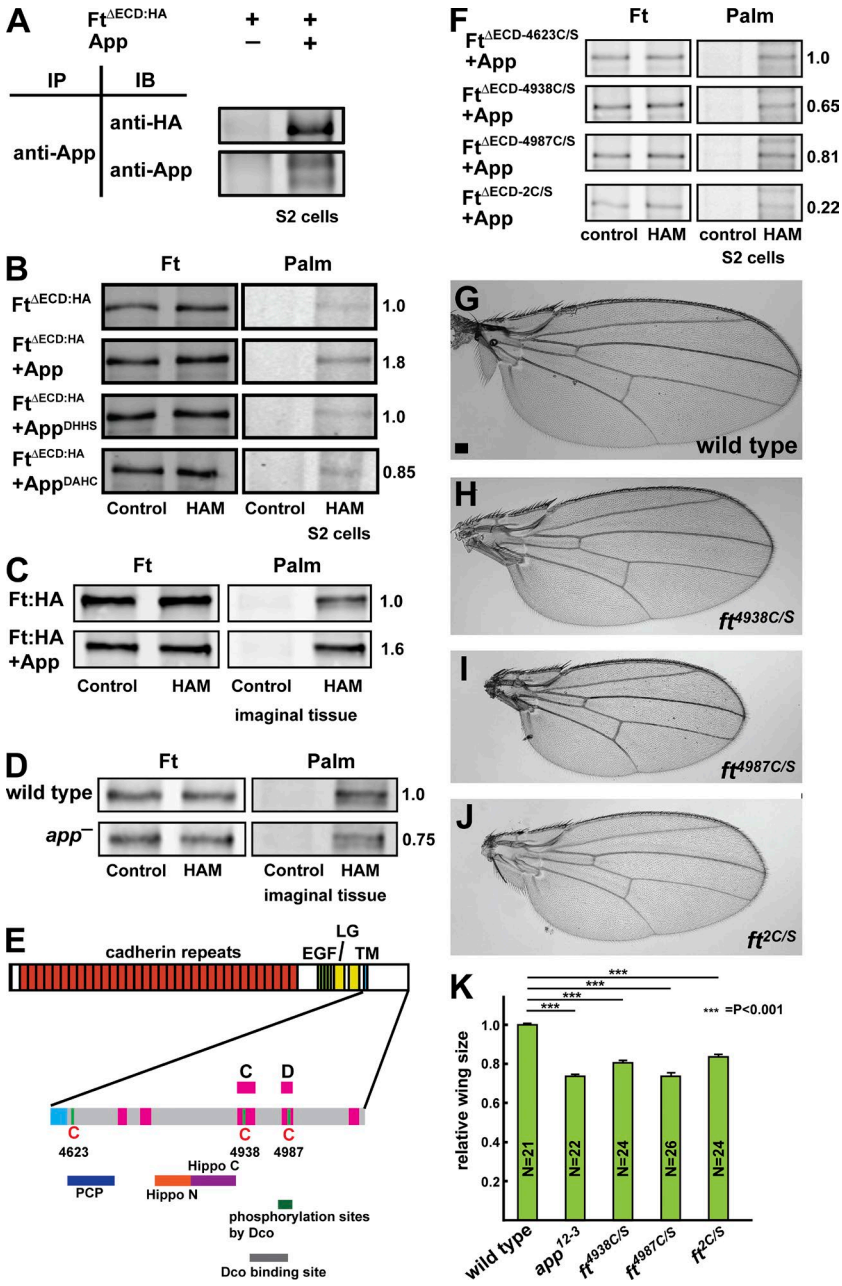

Figure 4. **Ft associates with and is palmitoylated by App.** (A) Coimmunoprecipitation between App and $Ft^{\Delta ECD}$ in S2 cells. (B) App promotes palmitoylation of Ft in S2 cells. Mutation of the App DHHC motif (App^{DHHS} or App^{DAHC}) blocks this effect. Palm, palmitoylation. (C and D) Ft is palmitoylated by App in imaginal disc epithelia. Bands shown represent the 110-kD C-terminal fragment of Ft, which includes the ICD, treated with phosphatase. Immunoprecipitated Ft is palmitoylated, and coexpression of App promotes increased palmitoylation (C). Palmitoylation of 110-kD Ft is reduced in app^{12-3} mutant imaginal discs (D). (E) The cysteine residues and functional domains in Ft-ICD (adapted from Matakatsu and Blair, 2012; Pan et al., 2013). The regions conserved between Ft and its human orthologue FAT atypical Cadherin 4 are shown in pink, and known functional domains are shown underneath. Conserved cysteine residues at 4,623, 4,938, and 4,987 are indicated. EGF, EGF-like domain; LG, Laminin G domain; TM, transmembrane domain. (F) Mapping of Ft palmitoylation sites using S2 cells. Mutation of Cys^{4623} ($Ft^{\Delta ECD\text{-}4623C/S}$) does not appear to affect Ft palmitoylation. Mutation of either Cys^{4938} ($Ft^{\Delta ECD\text{-}4938C/S}$) or Cys^{4987} ($Ft^{\Delta ECD\text{-}4987C/S}$) moderately decreases palmitoylation, whereas mutation of both together ($Ft^{\Delta ECD\text{-}2C/S}$) more severely affects palmitoylation (F). (G–K) Mutation of palmitoylated Cys residues in Ft results in decreased wing size. Representative wings from wild-type (G), $ft^{4938C/S}$ (H), $ft^{4987C/S}$ (I), and $ft^{2C/S}$ (J) adults. Mutation of Cys^{4938}, Cys^{4987}, or both together leads to undergrowth (K), consistent with activation of Ft. Error bars are mean ± SEM. ***, $P < 0.001$ (two-tailed unpaired Student's *t* test between wild type and each genotype). Bar, 100 µm.

and D) and in cells ectopically expressing a dominant-negative Dco protein (Rodrigues-Campos and Thompson, 2014). Similar effects were seen with other loss-of-function alleles (dco^{J3B9} and dco^{le88}; Fig. S1, G–I). Importantly, Dachs staining intensity in heterozygous dco^3/+ cells was intermediate between that of dco^3 homozygotes and wild type, suggesting that the level of Dco-driven Ft phosphorylation correlates with Dachs accumulation at the AJR in a linear fashion (Figs. 1 C and S1 I). In addition, Dachs protein levels in immunoblots were similarly affected by *dco* dosage (Fig. 1, H and I).

To elucidate the relationship between *app* and *dco* in regulating Ft, we examined genetic interactions between mutations in these genes. We first observed that heterozygosity for dco^3 suppressed the reduced size in wings homozygous for an *app* null allele (Fig. 6, A–D and G). In addition, although dco^3 homozygotes are completely lethal, *app* dco^3 double mutant animals survive until adulthood and have relatively normal-sized wings (Table S1 and Fig. 6, E and F). Consistent with these observations, the overgrowth phenotype of dco^3 imaginal discs is suppressed by *app* null alleles and by the app^{DHHS} and app^{DAHC} point mutants in the catalytic domain (Fig. 6, H–L; and not depicted). Together, these data strongly suggest that palmitoylation of the Ft-ICD by App antagonizes activation of Ft by Dco.

Given that Ft operates through Dachs to control growth, we asked whether the genetic antagonism we observed between *dco* and *app* affects Dachs localization. As described earlier (Fig. 1), Dachs is strongly localized to the AJR in *dco* mutant cells but is much more cytoplasmically distributed in *app* mutant cells. Accordingly, we wondered whether Dachs displays an intermediate distribution in *app dco* double mutant cells. Using somatic mosaics to generate double mutant clones in the background of each single mutant, we compared Dachs staining in *app* dco^3 cells to cells mutant for dco^3 or *app* alone. Consistent with their genetic antagonism, we found that removing *dco*

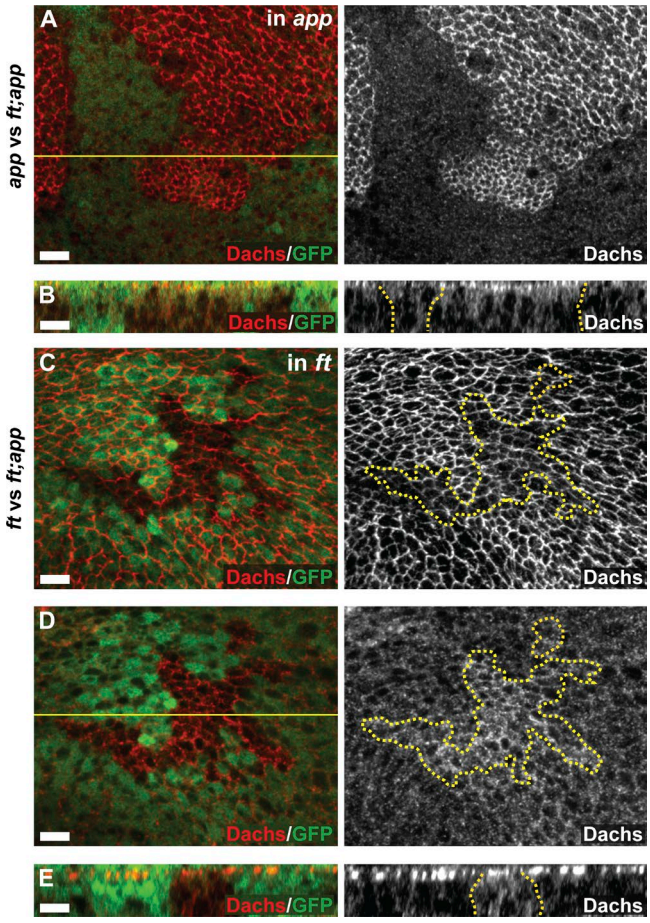

Figure 5. **App suppresses Ft and promotes Dachs accumulation at the AJR independently of Ft.** (A–E) Localization and level of Dachs in ft^{fd}; $app^{12\text{-}3}$ double mutant mitotic clones in comparison to $app^{12\text{-}3}$ (A and B) or $ft^{fd/Grv}$ (C–E) single mutant cells. Dachs is localized at the AJR in *ft; app* double mutant cells (A and B, right). This staining appears strong in comparison to *app* mutant cells (A, right), but weak in comparison to *ft* mutant cells (C, right), indicating that App promotes Dachs AJR accumulation even in the absence of Ft. The panels in A and C display maximum-intensity projections through the apical regions of wing cells. Double mutant mitotic clones indicated by absence of GFP. Bars, 5 µm.

in an *app* mutant background increased Dachs abundance at the AJR (Fig. 6, M and N), whereas removing *app* in a *dco* mutant background decreased Dachs at the AJR (Fig. 6, O and P). In addition, we noted that although dco^3 mutant cells displayed tightly junctional Dachs staining, removing App in addition caused increased cytoplasmic staining (Fig. 6, compare P to N bottom panels). Together, these experiments generated at least four distinct levels of Dachs junctional accumulation (*dco/dco* > *app dco/app dco* > *app dco/app* dco^+ > *app/app*) and suggest that palmitoylation by App functions antagonistically to phosphorylation by Dco to control Ft's ability to regulate Dachs.

Discussion

In this study, we sought to understand how Ft signaling is regulated by App, a palmitoyltransferase. Previous studies have shown that App acts together with Ft and Dachs to regulate growth, but the significance of App enzymatic activity, its substrates, and the mechanism by which it functions have not been clear (Matakatsu and Blair, 2008). Our results suggest a posttranslational mechanism for regulating the activity of Ft in growth control: the intracellular domain of Ft is palmitoylated by App, and palmitoylation negatively regulates Ft's ability to restrict tissue growth. This activity functions antagonistically to Dco, which activates Ft by phosphorylating its cytoplasmic tail. Independently, App also promotes Dachs accumulation at the AJR separate from its function as a palmitoyltransferase. We observed that App and Dachs form a complex when coexpressed in S2 cells, consistent with the idea that App, which localizes to the AJR, recruits Dachs through protein–protein association. Thus, we propose that App promotes growth both by restricting Ft's ability to repress Dachs and by directly promoting Dachs localization at the AJR. Together, these findings provide mechanistic insight into how App and Dco function to regulate Ft signaling and Dachs to control tissue growth (Fig. 7).

Regulation of the Ft ICD by posttranslational modifications

Previous studies have shown that interplay between phosphorylation and palmitoylation can regulate activity of transmembrane proteins by modulating interaction between their intracellular domain and the plasma membrane (Greaves and Chamberlain, 2007; Salaun et al., 2010). For example, the large conductance calcium- and voltage-gated potassium channel (BK channel) is both palmitoylated and phosphorylated within the intracellular STREX domain, which anchors the ICD to the inner face of the plasma membrane (Tian et al., 2008). Palmitoylation promotes STREX-mediated membrane association and channel activity, whereas phosphorylation by protein kinase A prevents membrane association and down-regulates the channel. Thus phosphorylation and palmitoylation act antagonistically and reversibly to regulate channel activity.

Our results suggest that palmitoylation and phosphorylation have similarly antagonistic effects on Ft activity in growth control. We demonstrated that the Ft ICD is palmitoylated at two conserved cysteine residues, Cys^{4938} and Cys^{4987}. CRISPR-mediated mutagenesis of these residues results in genetically activated *ft* alleles that suppress wing growth. Previous studies have shown that Dco binds to and phosphorylates Ft at a site adjacent to Cys^{4987}, the conserved "D domain," and that Dco promotes Ft's ability to restrict growth (Feng and Irvine, 2009; Sopko et al., 2009; Pan et al., 2013). The close proximity of the phosphorylation and palmitoylation sites on Ft suggest that these posttranslational modifications might compete with one another in regulating Ft activity. Consistent with that notion, we found that *app* mutations suppress the overgrowth and lethality phenotypes of dco^3, clear evidence of functional antagonism.

Based on the available data, we think it likely that posttranslational modifications affect Ft activity by modulating interactions of the Ft ICD with the plasma membrane, as previously proposed for other transmembrane proteins. Protein–protein interactions mediated by the ICD are likely affected by close association with the plasma membrane. The Ft D domain is known to interact with Fbxl7, a ubiquitin ligase that is thought to regulate Dachs stability and function (Bosch et al., 2014; Rodrigues-Campos and Thompson, 2014). Ft may also regulate Expanded, an upstream regulator of Hippo pathway activity, possibly through direct protein–protein interactions (Bennett and Harvey, 2006; Silva et al., 2006; Willecke et al., 2006; although see Feng and Irvine [2007] for an alternative view). Recent work has additionally demonstrated that the Ft

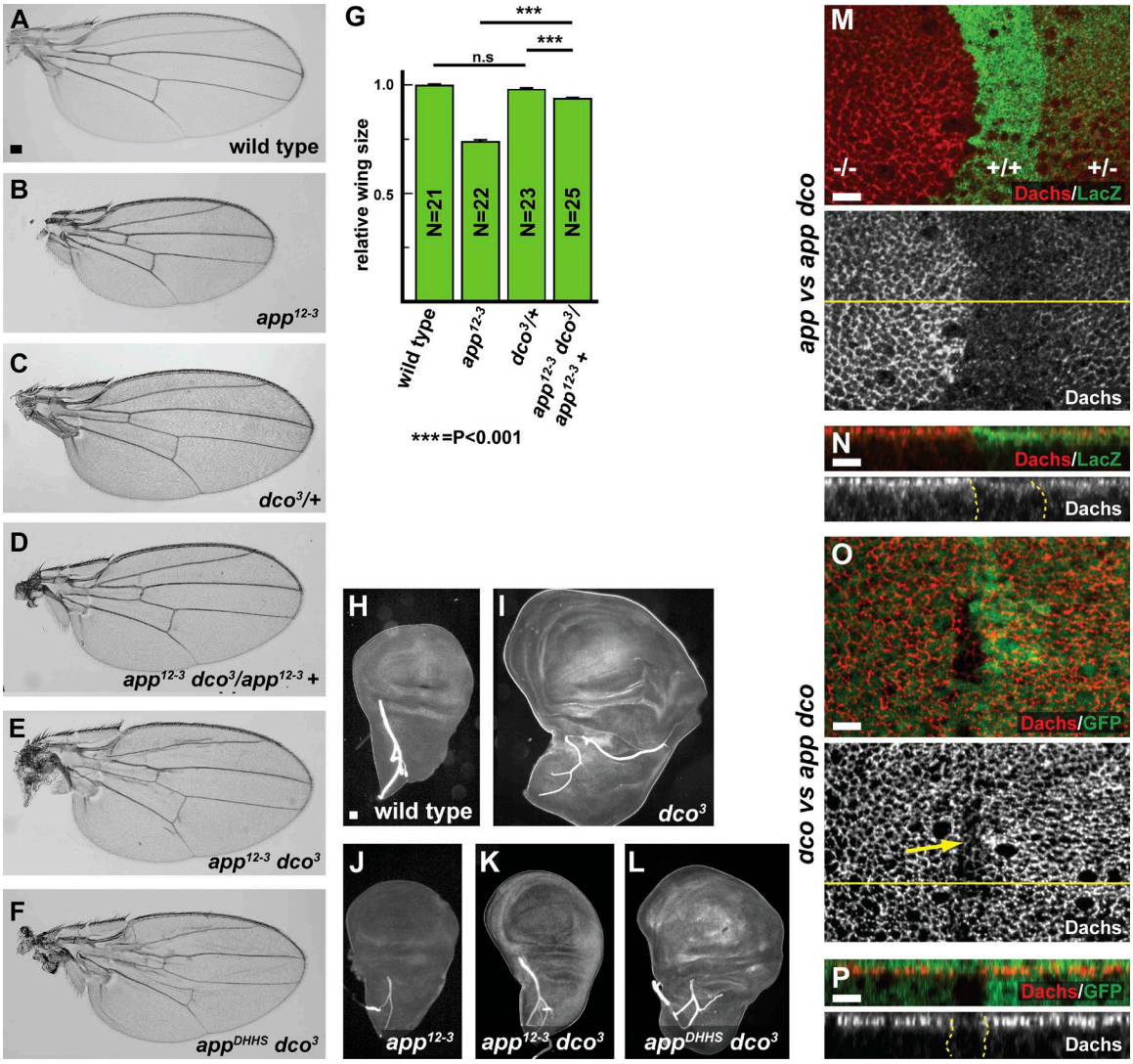

Figure 6. **App acts antagonistically to Dco.** (A–G) Genetic interactions between *dco* and *app* mutations in the adult wing. Representative wings from flies of the indicated genotypes. The small wing phenotype in $app^{12\text{-}3}$ adults is suppressed in flies heterozygous for the dco^3 allele (D, compare with B and C). $app^{12\text{-}3}$ dco^3 (E) and app^{DHHS} dco^3 (F) double mutants are viable and have almost normal wing size, whereas dco^3 single mutants are lethal (not depicted). Quantification of wing size is shown in G. Error bars are mean ± SEM. ***, $P < 0.001$ (two-tailed unpaired Student's *t* test between wild type and each genotype). n.s., not significant. (H–L) Genetic interactions between *dco* and *app* mutations in the wing imaginal discs. Representative wing discs from larvae of the indicated genotypes. Wing discs from dco^3 larvae display hyperplastic overgrowth (I), which is strongly suppressed in *app* dco^3 double mutant animals (compare K and L with I and J). (M–P) App and Dco antagonistically regulate Dachs accumulation at the AJR. Anti-Dachs staining in $app^{12\text{-}3}$ dco^3 mitotic clones in comparison to either $app^{12\text{-}3}$ (M and N) or dco^3 (O and P) single mutant cells. Dachs accumulates at the AJR at three detectably different levels according to *dco* dosage (+/+, +/−, and −/−) in the absence of *app* function (M and N). Similarly, at least two different levels of Dachs staining are seen with different *app* dosages in the absence of *dco* function (O and P; yellow arrow indicates double mutant clone). Note that together these panels display at least four detectably different Dachs levels at the AJR. Bars: (A) 100 µm; (H) 10 µm; (M–P) 5 µm.

ICD is cleaved and can translocate into mitochondria (Sing et al., 2014), a function that could also be affected by palmitoylation. Fully understanding all the functional implications of Ft palmitoylation will require further study.

An additional interesting implication of our model is that it predicts the possibility of multiple activity states for Ft that could be rapidly modulated by the interplay of phosphorylation–dephosphorylation and palmitoylation–depalmitoylation (Fig. 7). Our result showing that phosphatase treatment resolves palmitoylated Ft ICD to a single band (Fig. S5 C) indicates that palmitoylation and phosphorylation of the Ft ICD are not mutually exclusive and could occur independently. A possible implication of this observation is that these two posttranslational modifications act together to generate multiple levels of Ft activity in cells. Additionally, both phosphorylation and palmitoylation are reversible posttranslational modifications, suggesting a mechanism for precise and rapidly changeable regulation of growth in developing tissues.

Regulation of localization and level of Dachs at the AJR

Dachs functions downstream of Ft in growth control, and Dachs function in promoting growth depends on its ability to localize to the AJR (Mao et al., 2006). Using the anti-Dachs antisera described here, we have been able to examine the localization and abundance of endogenous Dachs under differing genotypes. In *app* null clones, Dachs fails to localize at the AJR and accumulates basally in disc epithelial cells. We

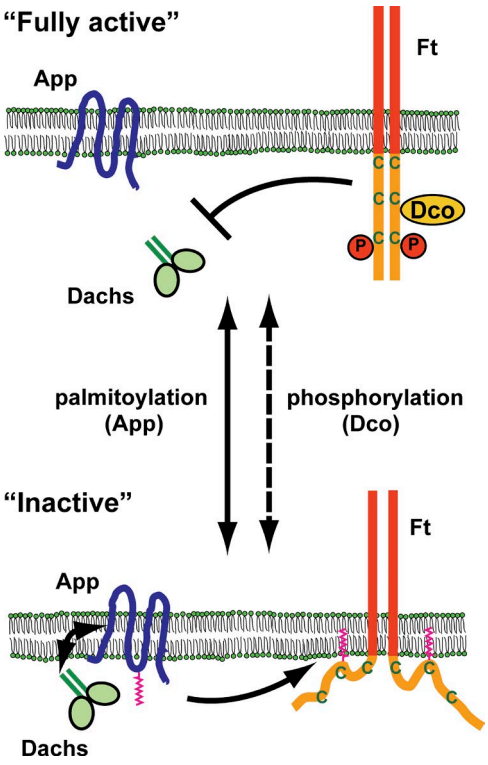

Figure 7. **A model for App function in Ft signaling.** Ft activity in repressing Dachs is regulated by two opposing posttranslational modifications: phosphorylation mediated by Dco and palmitoylation mediated by App. Dco phosphorylates and activates Ft. App suppresses Ft activity in part by palmitoylation and in part by recruiting Dachs to the AJR through forming a protein complex. Active Ft represses growth by preventing Dachs localization to the AJR. C, cysteine residue; P, phosphorylation.

observed that Dachs forms a complex with App when coexpressed in S2 cells, and we previously showed that coexpression of App with Dachs enhances the overgrowth phenotype of Dachs expression alone (Matakatsu and Blair, 2008). Together, these results are consistent with the model that App recruits Dachs to the AJR through protein–protein association. This function is independent of Ft palmitoylation, because (a) loss of App suppresses the *ft* null overgrowth phenotype (Matakatsu and Blair, 2008), and (b) we observed that Dachs is only partially mislocalized in cells carrying point mutations that disrupt App's palmitoyltransferase activity and in *ft* mutations that disrupt the target cysteine residues (unpublished data). Thus, our results suggest that App regulates Dachs function in two ways: by forming a complex with Dachs and recruiting it to the AJR, and by modulating activity of the Ft ICD. Additionally, Dachs recruitment to the AJR likely is regulated by other proteins because, in the absence of both Ft and App, some Dachs is still junctionally localized. Indeed, we found that App palmitoyltransferase activity is important even the absence of Ft (Fig. 2), and our recent work has identified a new component in Ft signaling, Dlish, that is also palmitoylated in an App-dependent manner (Zhang et al., 2016).

In addition to Dachs localization, our results suggest that its abundance also is an important factor. We observed that loss of Ft or Dco resulted in increased Dachs accumulation at the AJR and higher total Dachs levels in immunoblots, suggesting that Ft promotes Dachs degradation. However, loss of App, which activates Ft but results in mislocalization of Dachs, also results in increased overall Dachs levels. Collectively, these results suggest that Ft can only promote degradation of Dachs localized at the AJR. Two recent studies have shown that Ft binds Fbxl7, a component of the SCF complex that promotes protein degradation in the proteasome (Bosch et al., 2014; Rodrigues-Campos and Thompson, 2014). However, although one of these studies inferred from immunostaining that Fbxl7 regulates Dachs protein levels by promoting degradation of Dachs (Rodrigues-Campos and Thompson, 2014), the other demonstrated that Dachs protein levels in immunoblots are only slightly affected by loss of Fbxl7 (Bosch et al., 2014), a result that we confirmed (Fig. 1 I). Intriguingly, the D domain of Ft, which contains one of the Cys residues we have shown is necessary for palmitoylation, also is necessary for Fbxl7 binding to Ft (Bosch et al., 2014). However, Fbxl7 localization is not affected in *app* mutants (unpublished data), so it is unclear whether palmitoylation alters Ft–Fblx7 functional interactions. Further analysis of the relationship between Ft, Fbxl7, App, and Dachs could be informative in understanding how Ft regulates Dachs activity in growth control.

Ft signaling, palmitoylation, and cancer

Mutations in *Fat atypical cadherin 4* (*Fat4*), a mammalian *ft* orthologue, and *dachsous cadherin-related 1* (*Dchs1*) are both associated with Van Maldergem syndrome, a recessive disease associated with a wide range of neurological and other defects in humans (Cappello et al., 2013). Studies in mouse models of the disease have further shown that many of the associated phenotypes require Yap, a mammalian Yorkie orthologue, suggesting that these genes also operate upstream of the Hippo growth control pathway in mammals. Loss of *Fat4* function has also been implicated in tumorigenesis (Qi et al., 2009). It is not yet known whether mammalian Ft-related proteins are also palmitoylated, but we note that Cys^{4987} and adjacent residues in Ft are conserved in mammalian FAT4, suggesting this possibility. Characterization of conserved mechanisms such as palmitoylation that negatively regulate Ft function and therefore actively promote growth could provide potential targets for treatment of Hippo pathway–associated human disease.

Materials and methods

Fly genetics

To induce mitotic clones, larvae were treated at 37°C for 30 min in a water bath (Xu and Rubin, 1993). The following stocks were used: *ft^{fd} FRT40A/SM6-TM6b*; *$ft^{G\text{-}rv}$ FRT40A/SM6-TM6b*; *yw hs-FLP; ft^{fd} FRT40A; ubi-GFP 2AFRT/SM6-TM6*; *yw hs-FLP; ubi-GFP FRT40A; $app^{12\text{-}3}$ FRT2A/SM6-TM6b*; *ft^{fd} FRT40A; $app^{12\text{-}3}$ 2AFRT/SM6-TM6b*; *app^{e6} FRT2A/TM6b*; *$app^{12\text{-}3}$ FRT2A/TM6b*; *app^{DHHS} FRT2A/TM6b*; *app^{DAHC} FRT2A/TM6b*; *FRT82B dco^{3}/TM6b*; *FRT82B dco^{i3B9}/TM6b*; *FRT82B dco^{le88}/TM6b*; *$app^{12\text{-}3}$ FRT82B dco^{3}/TM6b*; *yw hs-FLP; $app^{12\text{-}3}$ FRT82B arm-lacZ/TM6b*; *yw hs-FLP; ubi-GFP 2AFRT dco^{3}/TM6b*; *d^{GC13} FRT40A/SM6-TM6b*; *$fbxl7^{Q201X}$ FRT82B/TM6b*; *yw hs-FLP; ubi-GFP FRT2A*; *yw hs-FLP; FRT82B arm-lacZ/SM6-TM6b*; *MS1096-gal4 UAS-FLP; FRT 82B hsp-CD2, y+, M(3)w124/TM2*; *yw hs-FLP; ubi-GFP FRT40A/SM6-TM6b*; *yw hs-FLP: arm-lacZ FRT40A/SM6-TM6b*; *ubi-GFP FRT40A fj-lacZ*; *UAS-ft:HA*; *UAS-app*; *UAS-app :GFP*; *UAS-app^{DHHS}*; *UAS-app^{DAHC}*; *UAS-dachs:V5*; *UAS-gish:Myc*; *UAS-zyxin:GFP*; *hh-gal4/TM6b*; *ban3-GFP hh-gal4/TM6b*; *ex-lacZ/CyO; ban3-GFP hh-gal4/TM2*; *tubulin-gal4/TM*; *da-gal4*; *y^{1} M{vas-Cas9.S}ZH-2A w^{1118}*; *nanos-Cas9*; and *w^{1118}*.

Quantification of wing sizes

Wings from 20 or more females for each genotype were mounted on glass slides in Permount (Thermo Fisher Scientific), and images were measured using ImageJ (National Institutes of Health).

Molecular cloning

Substitution mutations were introduced by using overlap extension PCR (Ho et al., 1989). For construction of *UAS-app^{DHHS}* and *UAS-app^{DAHC}*, the App coding sequence with mutations was amplified with PCR from *pUAS-app* (Matakatsu and Blair, 2008), cloned into pBluescript II SK, confirmed by DNA sequencing, and cloned into the EcoRI and XhoI sites of pUASt (Brand and Perrimon, 1993). For the Cys-to-Ser substitutions in Ft$^{\Delta ECD}$, Ft$^{\Delta ECD}$ with substitutions was amplified from *pUAS- Ft$^{\Delta ECD}$* (Matakatsu and Blair, 2006), cloned between the KpnI and NotI sites of pBluescript SKII, confirmed by DNA sequencing, and cloned into NotI–KpnI sites of pUASt.

Production of anti-Dachs antibodies

The DNA fragments corresponding to amino acids 1–280 (Dachs N) and 1,013–1,232 (Dachs C) were amplified from *UAS-dachs:V5* (Mao et al., 2006), cloned into pET28b (Invitrogen), and transformed into *Escherichia coli* BL 21(DE3). His-tagged proteins were induced with IPTG, purified with Ni-NTA resin (QIAGEN), dialyzed against PBS, and used to immunize rats (Panigen).

Immunostaining

Immunostaining of imaginal discs was performed as previously described (Matakatsu and Blair, 2004), except that fixations were performed in PBS with 2% formaldehyde for 5 min at RT. The following primary antibodies were used: rat anti–Dachs N and C (1:20,000), guinea pig anti-App (1:20,000; Matakatsu and Blair, 2008), mouse anti–β-galactosidase (1:1,000; Developmental Studies Hybridoma Bank), rabbit anti–β-galactosidase (1:1,000; Cappel), mouse anti-V5 (1:1,000; Invitrogen), and mouse anti-CD2 (1:1,000; Serotec). Images were taken using an LSM 880 confocal microscope (ZEISS; using Zen 2.1 software) or an Apotome (ZEISS) with an ORCA-ER CCD digital camera (Hamamatsu Photonics). Plan Apochromat 40×/1.4 and Plan Apochromat 63×/1.4 oil-immersion objectives (ZEISS) were used for LSM880. The acquired images were processed with ImageJ and Photoshop (Adobe Systems). Apical *z*-stacks were processed to make maximal projections using ImageJ.

Western blotting and immunoprecipitation

Transfections into S2 cells using dimethyldioctadecylammonium bromide (Sigma-Aldrich) were performed according to Han (1996). For immunoprecipitation, transfected S2 cells were harvested 72–96 h after transfection and resuspended in 500 µl lysis buffer (50 mM Tris, 150 mM NaCl, 5 mM EDTA, 0.02% NaN_3, 1% Triton X-100, 2 mM PMSF, and protease inhibitor, pH 7.4). After the samples were rotated for 1–2 h at 4°C, lysates were centrifuged at 14,000 rpm for 30 min at 4°C. Proteins were precipitated at 4°C overnight by adding suitable antibodies complexed to Protein A or G beads to the supernatant. After washing five times, precipitated proteins were eluted with SDS sample buffer. After separation of proteins by SDS-PAGE, they were transferred to nitrocellulose membranes (LI-COR Biosciences), immunostained according to the manufacturer, and detected using the LI-COR Biosciences imaging system (Odyssey CLx or Odyssey Infrared). To quantify Dachs protein, imaginal tissue from 10 wandering third-instar larvae was homogenized in 50 µl SDS sample buffer, and 5 µl of each lysate was used for SDS-PAGE. Dachs levels were measured using ImageJ. Mouse anti-αTubulin antibodies (1:20,000; Sigma-Aldrich) were used for normalization. Relative Dachs level for each genotype was quantified for at least four independent biological samples. The following primary antibodies were used: rat anti-Dachs (1:20,000), guinea pig anti-App (1:10,000; Matakatsu and Blair, 2008), rabbit anti-GFP (1:5,000; Abcam), rabbit anti–HA Y-11 (1:5,000; Santa Cruz Biotechnology, Inc.), mouse anti–Myc 9E10 (1:5,000; Santa Cruz Biotechnology, Inc.), rabbit anti-Myc (1:10,000; Cell Signaling Technology), and mouse anti–Flag M2 (1:20,000; Sigma-Aldrich).

Palmitoylation assays in vivo and in S2 cells

The palmitoylation assay was performed according to Drisdel and Green (2004). Imaginal tissues were dissected from 40 larvae or transfected S2 cells, homogenized, and suspended in 500 µl lysis buffer, pH 7.4, with 50 mM *N*-ethylmaleimide (Thermo Fisher Scientific). After rotating for 1–2 h at 4°C, lysates were centrifuged at 14,000 rpm for 20 min at 4°C. Proteins were precipitated overnight by adding suitable antibodies to the supernatant at 4°C followed by addition of protein A or G beads for 4 h at 4°C. Afterward, the beads were treated with 1 M hydroxylamine (pH 7.0–7.2) or 1 M Tris, labeled using 1.0 µM BMCC-biotin (Thermo Fisher Scientific) in lysis buffer, pH 6.2, for ∼1–2 h at 4°C, and eluted with SDS sample buffer. For some of the Ft palmitoylation assays, immunoprecipitated proteins were treated with lambda phosphatase (25°C for 30 min). Protein samples were run on 8% or 10% SDS-PAGE and transferred to nitrocellulose membranes (LI-COR Biosciences), and biotinylation was detected with IR Dye 800CW Streptavidin (LI-COR Biosciences). Quantification of Ft palmitoylation was performed by calculating the ratio of the Streptavidin channel to total Ft protein in the immunoprecipitation lane, and then expressed relative to control (either Ft$^{\Delta ECD}$ or Ft$^{\Delta ECD\text{-}4623C/S}$, depending on the experiment).

Gene editing with the CRISPR-Cas9 system

The target sequences for CRISPR mutagenesis were designed according to flyCRISPR Optimal Target Finder (http://tools.flycrispr.molbio.wisc.edu/targetFinder/). The target sequences were cloned into pU6-BbsI-chiRNA plasmid as described (Gratz et al., 2013; http://flycrispr.molbio.wisc.edu/protocols).

The indel mutagenesis used to generate null alleles and mutations in the DHHC motif in *app* is summarized in Fig. S2 (A and B). To obtain null alleles, the *app* gRNA#1 plasmid was injected into embryos expressing *vasa-Cas9* (Sebo et al., 2014). To obtain mutations in the App DHHC motif, *app* gRNA#2 and either a donor plasmid (for DHHS) or a single-stranded DNA oligonucleotide (for DAHC) were injected into embryos. To screen for *app* mutations, individual G0 flies were crossed to the hypomorphic *app^{1}* allele. Resultant *app* proximodistal patterning defects allowed ready identification of recombination or indel products. Candidates were further tested by NcoI digestion after PCR amplification of genomic DNA. Gene editing and ends-out replacements were confirmed by sequencing.

The gene editing steps for generating Cys-to-Ser mutations in *ft* are summarized in Fig. S5. To obtain *ft$^{4987C/S}$*, *ft*23gRNA plasmid and a mutagenic DNA oligonucleotide were coinjected into *vasa-Cas9* embryos. To obtain *ft$^{4938C/S}$* and *ft$^{2C/S}$*, plasmid DNA carrying the desired mutations and *ft*14gRNA were coinjected. After screening via restriction digestion, homologous recombination candidates were confirmed by sequencing.

Statistical analysis

Error bars indicate ± SEM in all graphs. Statistical analysis of wing size was performed using the two-tailed unpaired Student's *t* test. Statistical analysis of Dachs levels in Western blots was performed using the two-tailed paired Student's *t* test and the Wilcoxon rank sum test.

Online supplemental material

Fig. S1 shows the specificity of anti-Dachs antibodies and the localization of Dachs in *ft* mutant cells, when ectopically expressed, and in strong *dco* alleles. Fig. S2 describes the CRISPR-Cas9–induced *app* alleles and shows their PCP phenotypes. Fig. S3 shows the effects of ectopic expression of wild-type and mutant alleles of *app* on wing size, Dachs accumulation at the AJR, and the *ex-lacZ* Hippo reporter. Fig. S4 demonstrates that mutation of possible palmitoylation sites in Dachs does not significantly affect its function. Fig. S5 shows palmitoylation of Ft fragments and mutation of intracellular Cys residues in *ft* using CRISPR-Cas9. Table S1 shows the viability of *app*, *dco*, and double mutant allele combinations.

Acknowledgments

We thank K. Irvine, H. McNeill, J. Jiang, I. Hariharan, the Bloomington and Vienna Stock Centers, and the Developmental Studies Hybridoma Bank for reagents. We also thank C. Horth for technical assistance, W. Green and S. Antinone for advice on the palmitoylation assay, and members of the Fehon and Blair laboratories for critical comments throughout the course of this work.

This research was funded by National Institutes of Health grants NS034783 to R.G. Fehon and NS028202 to S.S. Blair.

The authors declare no competing financial interests.

Author contributions: Conceptualization and methodology, H. Matakatsu, S.S. Blair, and R.G. Fehon; investigation, H. Matakatsu; writing, original draft, H. Matakatsu and R.G. Fehon; writing, review and editing, H. Matakatsu, S.S. Blair, and R.G. Fehon.

Submitted: 20 September 2016
Revised: 19 November 2016
Accepted: 9 December 2016

References

Ambegaonkar, A.A., G. Pan, M. Mani, Y. Feng, and K.D. Irvine. 2012. Propagation of Dachsous-Fat planar cell polarity. *Curr. Biol.* 22:1302–1308. http://dx.doi.org/10.1016/j.cub.2012.05.049

Badouel, C., L. Gardano, N. Amin, A. Garg, R. Rosenfeld, T. Le Bihan, and H. McNeill. 2009. The FERM-domain protein Expanded regulates Hippo pathway activity via direct interactions with the transcriptional activator Yorkie. *Dev. Cell.* 16:411–420. http://dx.doi.org/10.1016/j.devcel.2009.01.010

Baumgartner, R., I. Poernbacher, N. Buser, E. Hafen, and H. Stocker. 2010. The WW domain protein Kibra acts upstream of Hippo in *Drosophila*. *Dev. Cell.* 18:309–316. http://dx.doi.org/10.1016/j.devcel.2009.12.013

Bennett, F.C., and K.F. Harvey. 2006. Fat cadherin modulates organ size in *Drosophila* via the Salvador/Warts/Hippo signaling pathway. *Curr. Biol.* 16:2101–2110. http://dx.doi.org/10.1016/j.cub.2006.09.045

Blair, S.S. 2012. Cell polarity: Overdosing on PCPs. *Curr. Biol.* 22:R567–R569. http://dx.doi.org/10.1016/j.cub.2012.06.044

Boggiano, J.C., and R.G. Fehon. 2012. Growth control by committee: Intercellular junctions, cell polarity, and the cytoskeleton regulate Hippo signaling. *Dev. Cell.* 22:695–702. http://dx.doi.org/10.1016/j.devcel.2012.03.013

Bosch, J.A., T.M. Sumabat, Y. Hafezi, B.J. Pellock, K.D. Gandhi, and I.K. Hariharan. 2014. The *Drosophila* F-box protein Fbxl7 binds to the protocadherin fat and regulates Dachs localization and Hippo signaling. *eLife.* 3:e03383. http://dx.doi.org/10.7554/eLife.03383

Bosveld, F., I. Bonnet, B. Guirao, S. Tlili, Z. Wang, A. Petitalot, R. Marchand, P.L. Bardet, P. Marcq, F. Graner, and Y. Bellaïche. 2012. Mechanical control of morphogenesis by Fat/Dachsous/Four-jointed planar cell polarity pathway. *Science.* 336:724–727. http://dx.doi.org/10.1126/science.1221071

Brand, A.H., and N. Perrimon. 1993. Targeted gene expression as a means of altering cell fates and generating dominant phenotypes. *Development.* 118:401–415.

Brittle, A., C. Thomas, and D. Strutt. 2012. Planar polarity specification through asymmetric subcellular localization of Fat and Dachsous. *Curr. Biol.* 22:907–914. http://dx.doi.org/10.1016/j.cub.2012.03.053

Cappello, S., M.J. Gray, C. Badouel, S. Lange, M. Einsiedler, M. Srour, D. Chitayat, F.F. Hamdan, Z.A. Jenkins, T. Morgan, et al. 2013. Mutations in genes encoding the cadherin receptor-ligand pair DCHS1 and FAT4 disrupt cerebral cortical development. *Nat. Genet.* 45:1300–1308. http://dx.doi.org/10.1038/ng.2765

Carvajal-Gonzalez, J.M., and M. Mlodzik. 2014. Mechanisms of planar cell polarity establishment in *Drosophila*. *F1000Prime Rep.* 6:98. http://dx.doi.org/10.12703/P6-98

Cho, E., Y. Feng, C. Rauskolb, S. Maitra, R. Fehon, and K.D. Irvine. 2006. Delineation of a Fat tumor suppressor pathway. *Nat. Genet.* 38:1142–1150. http://dx.doi.org/10.1038/ng1887

Drisdel, R.C., and W.N. Green. 2004. Labeling and quantifying sites of protein palmitoylation. *Biotechniques.* 36:276–285.

Drisdel, R.C., J.K. Alexander, A. Sayeed, and W.N. Green. 2006. Assays of protein palmitoylation. *Methods.* 40:127–134. http://dx.doi.org/10.1016/j.ymeth.2006.04.015

Enderle, L., and H. McNeill. 2013. Hippo gains weight: Added insights and complexity to pathway control. *Sci. Signal.* 6:re7. http://dx.doi.org/10.1126/scisignal.2004208

Feng, Y., and K.D. Irvine. 2007. Fat and expanded act in parallel to regulate growth through warts. *Proc. Natl. Acad. Sci. USA.* 104:20362–20367. http://dx.doi.org/10.1073/pnas.0706722105

Feng, Y., and K.D. Irvine. 2009. Processing and phosphorylation of the Fat receptor. *Proc. Natl. Acad. Sci. USA.* 106:11989–11994. http://dx.doi.org/10.1073/pnas.0811540106

Fukata, Y., and M. Fukata. 2010. Protein palmitoylation in neuronal development and synaptic plasticity. *Nat. Rev. Neurosci.* 11:161–175. http://dx.doi.org/10.1038/nrn2788

Genevet, A., M.C. Wehr, R. Brain, B.J. Thompson, and N. Tapon. 2010. Kibra is a regulator of the Salvador/Warts/Hippo signaling network. *Dev. Cell.* 18:300–308. http://dx.doi.org/10.1016/j.devcel.2009.12.011

Gratz, S.J., A.M. Cummings, J.N. Nguyen, D.C. Hamm, L.K. Donohue, M.M. Harrison, J. Wildonger, and K.M. O'Connor-Giles. 2013. Genome engineering of *Drosophila* with the CRISPR RNA-guided Cas9 nuclease. *Genetics.* 194:1029–1035. http://dx.doi.org/10.1534/genetics.113.152710

Greaves, J., and L.H. Chamberlain. 2007. Palmitoylation-dependent protein sorting. *J. Cell Biol.* 176:249–254. http://dx.doi.org/10.1083/jcb.200610151

Halder, G., and R.L. Johnson. 2011. Hippo signaling: Growth control and beyond. *Development.* 138:9–22. http://dx.doi.org/10.1242/dev.045500

Hamaratoglu, F., M. Willecke, M. Kango-Singh, R. Nolo, E. Hyun, C. Tao, H. Jafar-Nejad, and G. Halder. 2006. The tumour-suppressor genes NF2/Merlin and Expanded act through Hippo signalling to regulate cell proliferation and apoptosis. *Nat. Cell Biol.* 8:27–36. http://dx.doi.org/10.1038/ncb1339

Han, K. 1996. An efficient DDAB-mediated transfection of *Drosophila* S2 cells. *Nucleic Acids Res.* 24:4362–4363. http://dx.doi.org/10.1093/nar/24.21.4362

Hariharan, I.K. 2015. Organ size control: Lessons from *Drosophila*. *Dev. Cell.* 34:255–265. http://dx.doi.org/10.1016/j.devcel.2015.07.012

Ho, S.N., H.D. Hunt, R.M. Horton, J.K. Pullen, and L.R. Pease. 1989. Site-directed mutagenesis by overlap extension using the polymerase chain reaction. *Gene.* 77:51–59. http://dx.doi.org/10.1016/0378-1119(89)90358-2

Lawrence, P.A., and J. Casal. 2013. The mechanisms of planar cell polarity, growth and the Hippo pathway: Some known unknowns. *Dev. Biol.* 377:1–8. http://dx.doi.org/10.1016/j.ydbio.2013.01.030

Linder, M.E., and R.J. Deschenes. 2007. Palmitoylation: Policing protein stability and traffic. *Nat. Rev. Mol. Cell Biol.* 8:74–84. http://dx.doi.org/10.1038/nrm2084

Ling, C., Y. Zheng, F. Yin, J. Yu, J. Huang, Y. Hong, S. Wu, and D. Pan. 2010. The apical transmembrane protein Crumbs functions as a tumor suppressor that regulates Hippo signaling by binding to Expanded. *Proc. Natl. Acad. Sci. USA.* 107:10532–10537. http://dx.doi.org/10.1073/pnas.1004279107

Lobo, S., W.K. Greentree, M.E. Linder, and R.J. Deschenes. 2002. Identification of a Ras palmitoyltransferase in *Saccharomyces cerevisiae*. *J. Biol. Chem.* 277:41268–41273. http://dx.doi.org/10.1074/jbc.M206573200

Ma, D., C.H. Yang, H. McNeill, M.A. Simon, and J.D. Axelrod. 2003. Fidelity in planar cell polarity signalling. *Nature.* 421:543–547. http://dx.doi.org/10.1038/nature01366

Mao, Y., C. Rauskolb, E. Cho, W.L. Hu, H. Hayter, G. Minihan, F.N. Katz, and K.D. Irvine. 2006. Dachs: An unconventional myosin that functions downstream of Fat to regulate growth, affinity and gene expression in *Drosophila*. *Development.* 133:2539–2551. http://dx.doi.org/10.1242/dev.02427

Matakatsu, H., and S.S. Blair. 2004. Interactions between Fat and Dachsous and the regulation of planar cell polarity in the *Drosophila* wing. *Development.* 131:3785–3794. http://dx.doi.org/10.1242/dev.01254

Matakatsu, H., and S.S. Blair. 2006. Separating the adhesive and signaling functions of the Fat and Dachsous protocadherins. *Development.* 133:2315–2324. http://dx.doi.org/10.1242/dev.02401

Matakatsu, H., and S.S. Blair. 2008. The DHHC palmitoyltransferase approximated regulates Fat signaling and Dachs localization and activity. *Curr. Biol.* 18:1390–1395. http://dx.doi.org/10.1016/j.cub.2008.07.067

Matakatsu, H., and S.S. Blair. 2012. Separating planar cell polarity and Hippo pathway activities of the protocadherins Fat and Dachsous. *Development.* 139:1498–1508. http://dx.doi.org/10.1242/dev.070367

Matis, M., and J.D. Axelrod. 2013. Regulation of PCP by the Fat signaling pathway. *Genes Dev.* 27:2207–2220. http://dx.doi.org/10.1101/gad.228098.113

Mitchell, D.A., G. Mitchell, Y. Ling, C. Budde, and R.J. Deschenes. 2010. Mutational analysis of *Saccharomyces cerevisiae* Erf2 reveals a two-step reaction mechanism for protein palmitoylation by DHHC enzymes. *J. Biol. Chem.* 285:38104–38114. http://dx.doi.org/10.1074/jbc.M110.169102

Pan, G., Y. Feng, A.A. Ambegaonkar, G. Sun, M. Huff, C. Rauskolb, and K.D. Irvine. 2013. Signal transduction by the Fat cytoplasmic domain. *Development.* 140:831–842. http://dx.doi.org/10.1242/dev.088534

Qi, C., Y.T. Zhu, L. Hu, and Y.J. Zhu. 2009. Identification of Fat4 as a candidate tumor suppressor gene in breast cancers. *Int. J. Cancer.* 124:793–798. http://dx.doi.org/10.1002/ijc.23775

Ren, J., L. Wen, X. Gao, C. Jin, Y. Xue, and X. Yao. 2008. CSS-Palm 2.0: An updated software for palmitoylation sites prediction. *Protein Eng. Des. Sel.* 21:639–644. http://dx.doi.org/10.1093/protein/gzn039

Rodrigues-Campos, M., and B.J. Thompson. 2014. The ubiquitin ligase FbxL7 regulates the Dachsous-Fat-Dachs system in *Drosophila*. *Development.* 141:4098–4103. http://dx.doi.org/10.1242/dev.113498

Rogulja, D., C. Rauskolb, and K.D. Irvine. 2008. Morphogen control of wing growth through the Fat signaling pathway. *Dev. Cell.* 15:309–321. http://dx.doi.org/10.1016/j.devcel.2008.06.003

Roth, A.F., Y. Feng, L. Chen, and N.G. Davis. 2002. The yeast DHHC cysteine-rich domain protein Akr1p is a palmitoyl transferase. *J. Cell Biol.* 159:23–28. http://dx.doi.org/10.1083/jcb.200206120

Salaun, C., J. Greaves, and L.H. Chamberlain. 2010. The intracellular dynamic of protein palmitoylation. *J. Cell Biol.* 191:1229–1238. http://dx.doi.org/10.1083/jcb.201008160

Sebo, Z.L., H.B. Lee, Y. Peng, and Y. Guo. 2014. A simplified and efficient germline-specific CRISPR/Cas9 system for *Drosophila* genomic engineering. *Fly (Austin).* 8:52–57. http://dx.doi.org/10.4161/fly.26828

Silva, E., Y. Tsatskis, L. Gardano, N. Tapon, and H. McNeill. 2006. The tumor-suppressor gene fat controls tissue growth upstream of expanded in the hippo signaling pathway. *Curr. Biol.* 16:2081–2089. http://dx.doi.org/10.1016/j.cub.2006.09.004

Sing, A., Y. Tsatskis, L. Fabian, I. Hester, R. Rosenfeld, M. Serricchio, N. Yau, M. Bietenhader, R. Shanbhag, A. Jurisicova, et al. 2014. The atypical cadherin fat directly regulates mitochondrial function and metabolic state. *Cell.* 158:1293–1308. http://dx.doi.org/10.1016/j.cell.2014.07.036

Sopko, R., E. Silva, L. Clayton, L. Gardano, M. Barrios-Rodiles, J. Wrana, X. Varelas, N.I. Arbouzova, S. Shaw, S. Saburi, et al. 2009. Phosphorylation of the tumor suppressor fat is regulated by its ligand Dachsous and the kinase discs overgrown. *Curr. Biol.* 19:1112–1117. http://dx.doi.org/10.1016/j.cub.2009.05.049

Staley, B.K., and K.D. Irvine. 2012. Hippo signaling in *Drosophila*: recent advances and insights. *Dev. Dyn.* 241:3–15. http://dx.doi.org/10.1002/dvdy.22723

Thomas, C., and D. Strutt. 2012. The roles of the cadherins Fat and Dachsous in planar polarity specification in *Drosophila*. *Dev. Dyn.* 241:27–39. http://dx.doi.org/10.1002/dvdy.22736

Tian, L., O. Jeffries, H. McClafferty, A. Molyvdas, I.C. Rowe, F. Saleem, L. Chen, J. Greaves, L.H. Chamberlain, H.G. Knaus, et al. 2008. Palmitoylation gates phosphorylation-dependent regulation of BK potassium channels. *Proc. Natl. Acad. Sci. USA.* 105:21006–21011. http://dx.doi.org/10.1073/pnas.0806700106

Vrabioiu, A.M., and G. Struhl. 2015. Fat/Dachsous signaling promotes *Drosophila* wing growth by regulating the conformational state of the NDR kinase Warts. *Dev. Cell.* 35:737–749. http://dx.doi.org/10.1016/j.devcel.2015.11.027

Willecke, M., F. Hamaratoglu, M. Kango-Singh, R. Udan, C.L. Chen, C. Tao, X. Zhang, and G. Halder. 2006. The fat cadherin acts through the hippo tumor-suppressor pathway to regulate tissue size. *Curr. Biol.* 16:2090–2100. http://dx.doi.org/10.1016/j.cub.2006.09.005

Xu, T., and G.M. Rubin. 1993. Analysis of genetic mosaics in developing and adult *Drosophila* tissues. *Development.* 117:1223–1237.

Yu, J., Y. Zheng, J. Dong, S. Klusza, W.M. Deng, and D. Pan. 2010. Kibra functions as a tumor suppressor protein that regulates Hippo signaling in conjunction with Merlin and Expanded. *Dev. Cell.* 18:288–299. http://dx.doi.org/10.1016/j.devcel.2009.12.012

Yue, T., A. Tian, and J. Jiang. 2012. The cell adhesion molecule echinoid functions as a tumor suppressor and upstream regulator of the Hippo signaling pathway. *Dev. Cell.* 22:255–267. http://dx.doi.org/10.1016/j.devcel.2011.12.011

Zhang, Y., X. Wang, H. Matakatsu, R. Fehon, and S.S. Blair. 2016. The novel SH3 domain protein Dlish/CG10933 mediates fat signaling in *Drosophila* by binding and regulating Dachs. *eLife.* 5:e16624. http://dx.doi.org/10.7554/eLife.16624

Zilian, O., E. Frei, R. Burke, D. Brentrup, T. Gutjahr, P.J. Bryant, and M. Noll. 1999. Double-time is identical to discs overgrown, which is required for cell survival, proliferation and growth arrest in *Drosophila* imaginal discs. *Development.* 126:5409–5420.